

Light-induced multiple electronic-state coupling of O_2^+ in intense laser fields

Akiyoshi Hishikawa, Shilin Liu,^{a)} Atsushi Iwasaki, and Kaoru Yamanouchi^{b)}

Department of Chemistry, School of Science, The University of Tokyo, 7-3-1 Hongo, Bunkyo-ku, Tokyo 113-0033, Japan

(Received 18 January 2001; accepted 8 March 2001)

The dissociation processes, $O_2^+ \rightarrow O^+ + O$, in intense laser fields (100 fs, $\sim 3 \times 10^{14}$ W/cm²) are studied at the laser wavelength of 795 and 398 nm on the basis of the momentum imaging maps of the O^+ fragment ions. The covariance map measurements are performed with high momentum resolution to assign securely the dissociation pathways. From the anisotropic momentum distribution of O^+ with respect to the laser polarization direction, the electronic states of O_2^+ are found to be coupled exclusively through parallel transitions in the course of the dissociation process. The released kinetic energy of O^+ for both 795 and 398 nm are interpreted consistently by a sequential coupling model of light-dressed potential curves of O_2^+ in the quartet Π state manifold.

© 2001 American Institute of Physics. [DOI: 10.1063/1.1368383]

I. INTRODUCTION

When the magnitude of a light–molecule interaction exceeds a perturbative regime, interatomic potentials of a molecule are substantially deformed by the light fields. The resultant light-deformed potentials lead to a new class of molecular phenomena such as bond-softening, bond-hardening, and above-threshold dissociation (ATD).¹ For a one-electron system, H_2^+ , these phenomena have been interpreted well in terms of the light-dressed picture consisting of the two lowest electronic states, $1s\sigma_g$ and $2p\sigma_u$, both of which are well separated energetically from higher lying electronic states.^{1,2} It has been revealed through theoretical calculations^{3,4} that the strong coupling between these electronic states is crucial for ionization of H_2^+ in intense laser fields, which occurs most efficiently at a critical internuclear distance $R_c \sim 10$ a.u.³

As for *multielectron* molecules, the main concern in previous literature has been the multiple-ionization process followed by a bond fission process called the Coulomb explosion occurring at higher field intensities (1–10 PW/cm²; 1 PW = 10^{15} W).^{5,6} The observed enhancement of the ionization rates at a critical distance has been successfully explained by a classical field ionization model, where the role of electronic states is not taken into account explicitly. On the other hand, recent studies on triatomic molecules^{7–12} have revealed that they undergo ultrafast structural deformation in such a high laser-field intensity and that this could be interpreted by the formation of the light-deformed potentials prior to the Coulomb explosion.^{9–12} However, such light-induced potential deformation in a multielectron molecule could not be explained by a simple picture in which only two electronic states are coupled with each other as in the case of

H_2^+ , because a multiple coupling would be induced among a number of electronic states with high density.

In the present study, we report definitive evidence of such a multiple coupling among more than two electronic states of O_2^+ in intense laser fields (~ 0.3 PW/cm²), through the measurements of the momentum vector distribution of the O^+ fragment ions produced from the bond-breaking process of $O_2^+ \rightarrow O^+ + O$.

II. EXPERIMENT

The amplified ultrashort laser pulses (795 nm, 100 fs, ~ 1 mJ) generated by a regenerative amplifier system (BMI alpha 10) were focused by a quartz lens ($f = 150$ mm) to produce intense laser fields (~ 0.3 PW/cm²). The second harmonics (398 nm) was generated by a BBO crystal plate of 1 mm thickness. The mass-resolved momentum imaging (MRMI) maps of O^+ produced from O_2 were constructed from the time-of-flight (TOF) mass spectra recorded by an oscilloscope (LeCroy 9370) at 18 different angles of the laser polarization vector with respect to the TOF detection axis in the range between 0° and 180°. The momentum p_{\parallel} of the ejected fragments along the TOF axis is derived by using a formula, $p_{\parallel} = qF\Delta T$, where ΔT is half of the difference in the flight time between the fragments ejected in forward and backward directions, q is the charge of the fragment ion, and F is the static electric field applied for the ion extraction.

A small aperture (10 mm ϕ) was placed in front of the microchannel plate (MCP) ion detector to achieve high momentum resolution. The pressure in the vacuum chamber was set in the range between 6×10^{-8} and 2×10^{-7} Torr depending on the laser-field intensity to avoid a space charge effect. The energies of the respective laser pulses were monitored by a single channel analyzer, which supplies trigger signals to the oscilloscope. The laser spot size at the focal spot was measured by projecting its image onto a charge coupled device camera through an objective lens (10 \times) to be 6.4×10^2 and 1.3×10^3 μm^2 for 795 and 398 nm, respectively.

^{a)}Permanent address: Department of Chemical Physics, University of Science and Technology of China, Hefei, Anhui 230026, China.

^{b)}Author to whom correspondence should be addressed; electronic mail: kaoru@chem.s.u-tokyo.ac.jp

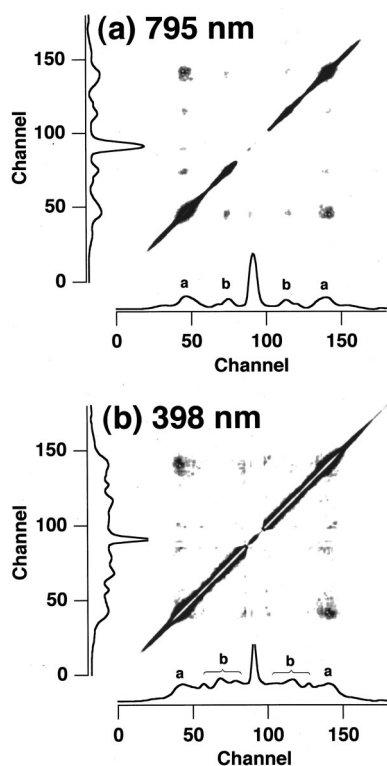


FIG. 1. The TOF mass spectrum and the covariance map of O^+ (one channel=1 ns) at (a) $\lambda \sim 795$ nm, 0.4 PW/cm^2 and (b) $\lambda \sim 398$ nm 0.7 PW/cm^2 , obtained for 3×10^4 laser shots. The raw signal intensity corresponding to O_2^{2+} is multiplied by a factor of 0.2 in order to reduce false coincidence signals originating from its strong intensity.

In order to discriminate the (1,0) dissociation process $O_2^+ \rightarrow O^+ + O$ from the (1,1) Coulomb explosion process $O_2^{2+} \rightarrow O^+ + O^+$, both of which could appear in the MRMI map of O^+ , the correlation between the O^+ fragments was measured by the covariance map technique.¹³ The covariance map was measured after accumulation of more than 3×10^4 shots of laser pulses. The pressure in the chamber was reduced as low as 8×10^{-8} Torr to keep the ion count rate less than 50 ions/shot. The other experimental conditions were the same as those in the MRMI measurements. Under the present experimental conditions, false covariance signals appeared between O^+ ions and O_2^{2+} ions whose magnitude is substantially larger than the O^+ signal (see Fig. 1). In order to reduce such an artifact, the raw signal intensities of O_2^{2+} were multiplied by a factor of 0.2 in the construction of the covariance map.

III. RESULTS AND DISCUSSION

A. Assignment of the dissociation pathways

The observed TOF mass spectra and the covariance map of O^+ recorded at $\lambda \sim 795$ nm with the laser polarization vector parallel to the TOF axis are shown in Fig. 1(a). The sharp peak observed at the center of the TOF mass spectra is attributed to O_2^{2+} having the same mass-to-charge ratio as O^+ . A pair of peaks labeled with a corresponds to the O^+ ions ejected in the forward and backward directions with respect to the MCP ion detector. The positive covariance

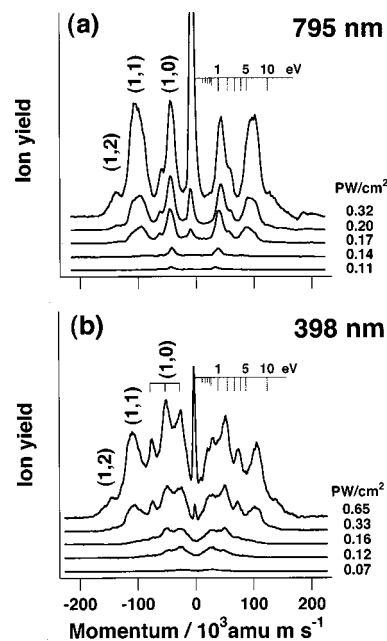


FIG. 2. The laser-field dependence of the one-dimensional cut of the MRMI maps of O^+ (Fig. 1) along the laser polarization direction for 795 nm (a) and 398 nm (b). The energy scale (in eV) shows the total released kinetic energy.

signals between these forward and backward peaks in the covariance map [Fig. 1(a)] indicate that these components are produced in a correlated manner through the (1,1) Coulomb explosion process,¹⁴ $O_2^{2+} \rightarrow O^+ + O^+$.

Another pair of peaks labeled with b with a small shoulderlike structure on the higher momentum side is seen in the TOF spectrum in Fig. 1(a), exhibiting a marked contrast with N_2 (Ref. 15) and NO ,¹⁶ whose TOF spectra showed no clear feature in the smaller momentum region inside the (1,1) pathway. The covariance map of O^+ showing no distinct correlation in the small momentum region implies that these slow O^+ ions are produced with a neutral O atom as a counterpart fragment through the (1,0) dissociation pathway, $O_2^+ \rightarrow O^+ + O$. Existence of such low kinetic energy components of O^+ from O_2 in intense laser fields was observed previously by Normand *et al.*¹⁴ with lower momentum resolution at $\lambda \sim 610$ and 305 nm, and were also assigned to the (1,0) pathway.

The (1,0) component is clearly identified at low laser-field intensities ($\sim 0.1 \text{ PW/cm}^2$) as shown in Fig. 2(a), while the (1,1) component becomes prominent at a higher field intensity ($\sim 0.17 \text{ PW/cm}^2$). The field-intensity dependence shows that the (1,1) Coulomb explosion pathway is composed of two distinct features at 90×10^3 and $105 \times 10^3 \text{ amu m/s}$. By increasing the field intensity further, another pair of peaks appears at the momentum of $140 \times 10^3 \text{ amu m/s}$, originating from the (1,2) Coulomb explosion process, $O_2^{3+} \rightarrow O^+ + O^{2+}$. The lower appearance intensity of the (1,0) component rather than that of the (1,1) component confirms these assignments of the dissociation pathways because a lower charge state of parent molecular ions should be produced with a lower appearance intensity. The present assignment of the (1,0) component is also sup-

TABLE I. The total kinetic energies of O^+ released through $O_2^+ \rightarrow O^+ + O$ in intense laser fields (~ 0.1 PW/cm²). The calculated values are derived from the interaction sequence within the quartet-II manifold.

795 nm ^a		398 nm ^a		610 nm ^b		305 nm ^c	
Obs.	Calc.	Obs.	Calc.	Obs.	Calc.	Obs.	Calc.
1.1(1)	0.8(2)	0.5(1)	0.6(2)	0.72(10) ^d	0.7(2)	0.52(6)	—
2.0(2)	—	1.8(2)	1.7(2)	1.36(20) ^d	2.1(2)	1.04(10)	—
...	...	3.7(2)	3.6(2)	2.60(30)	—	1.94(20)	1.5(2)

^aPresent work. The laser pulse duration is $\tau \sim 100$ fs.

^bReference 14 ($\tau \sim 2$ ps).

^cReference 14 ($\tau \sim 1.4$ ps).

^dDominant at a weak field intensity (0.05 PW/cm²).

ported by the measurement of the saturation intensity. From the O^+ yield plotted as a function of the laser field intensity in the 0.1–0.7 PW/cm² range, the saturation intensity of the O^+ component is estimated to be 0.2(5) PW/cm². The agreement of the saturation intensity with that of O_2^+ , 0.2 PW/cm², which we estimated from the ion yield curve obtained by Guo *et al.*¹⁷ at 800 nm, indicates that the slow O^+ ions are produced almost simultaneously with the formation of O_2^+ ion.

The sharp (1,0) peak suggests that only a limited number of the electronic states are involved in the fragmentation process at this field intensity. Since the parent O_2^+ ions are expected to be prepared in its *bound* low-lying electronic states such as $X^2\Pi_g^-$ or $a^4\Pi_u$ by a removal of one electron from the triplet ground state ($X^3\Sigma_g^-$) of O_2 , the dissociation should proceed through a coupling with higher-lying *repulsive* electronic states. If nonresonant multiphoton ionization is assumed, the $X^2\Pi_g^-$ state of O_2^+ would be prepared in its low vibrational levels, $v \leq 5$, determined by the Franck–Condon overlap with respect to the $X^3\Sigma_g^-$ state of O_2 . On the other hand, when O_2^+ is produced in the $a^4\Pi_u$ state, O_2^+ can be prepared in the vibrational levels of $0 \leq v \leq 18$, because of the wide Franck–Condon region attained by the large displacement of the equilibrium internuclear distance ($R_e = 1.3813 \text{ \AA}$)¹⁸ of the $a^4\Pi_u$ state from $R_e = 1.20752 \text{ \AA}$ ¹⁸ of O_2 in the $X^3\Sigma_g^-$ state.

The TOF spectrum of O^+ at $\lambda \sim 398$ nm [Figs. 1(b) and 2(b)] exhibits a marked difference from that observed at $\lambda \sim 795$ nm. In addition to the features for the (1,1) Coulomb explosion pathway labeled with a, three pairs of peaks [labeled with b] are observed in the momentum region below 70×10^3 amu m/s. Based on the covariance map shown in Fig. 1(b), which exhibits no clear correlation signal for the three features, three peaks are all assigned to the (1,0) dissociation pathway. The kinetic energies released through the (1,0) pathway at two different wavelengths, $\lambda \sim 795$ and 398 nm, are determined from the peaks observed in the momentum distributions in Fig. 2 and are summarized in Table I.

B. Anisotropic fragment distribution

The observed MRMI map for O^+ recorded at $\lambda \sim 795$ nm is shown in Fig. 3(a), together with the assignments of the dissociation pathways established above. The (1,0) pathway in the MRMI map exhibits a large anisotropy along the di-

rection of the laser polarization. As shown in Fig. 3(b), an anisotropic ejection of the O^+ fragment along the laser polarization direction is also identified for the three (1,0) features in the MRMI map observed at 398 nm. In this MRMI map, an isotropic component with broad momentum distribution with a width of 17×10^3 amu ms⁻¹ can be seen along the circle with a momentum radius of 26×10^3 amu ms⁻¹.

In the ultrafast photodissociation of a diatomic molecule, the fragment anisotropy is determined by the direction of the transition moment (μ) with respect to the molecular axis (z).¹⁹ When $\mu \parallel z$ (parallel transition), the angular distribution of the fragment in the space-fixed frame $P(\theta)$ is expressed as $P(\theta) \propto \cos^2 \theta$, while in the perpendicular transition ($\mu \perp z$), $P(\theta) \propto \sin^2 \theta$, where θ is defined as an angle between the laser polarization direction and the direction of the molecular axis.

In the case of a multiphoton transition, the fragment anisotropy can be expressed by a product of these distribution functions $P(\theta) \propto \cos^{2m} \theta \sin^{2n} \theta$, where m and n represent, re-

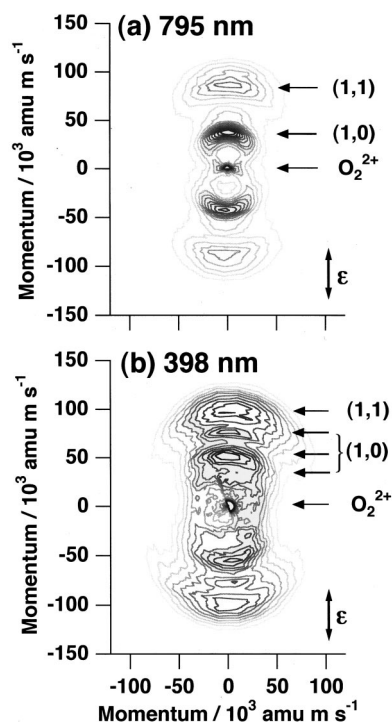


FIG. 3. The MRMI maps of O^+ produced from O_2 in intense laser fields: (a) $\lambda \sim 795$ nm, 0.2 PW/cm², (b) $\lambda \sim 398$ nm, 0.6 PW/cm². The laser polarization vector (ϵ) is indicated with an arrow.

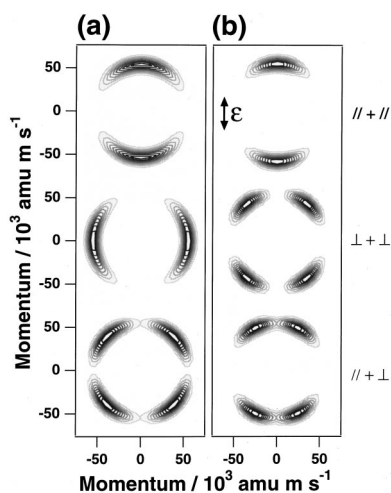


FIG. 4. The simulated MRMI maps for a fragment ion with a peak momentum of $\sim 50 \times 10^3$ amu m/s produced through a two-photon absorption: In (a), an isotropic distribution of the molecular axis is assumed for parent molecules. In (b), a prealigned distribution of parent molecules with $P(\theta) = \cos^6 \theta$ with respect to the laser polarization direction is assumed. The laser polarization vector (ϵ) is indicated with an arrow.

spectively, the number of parallel transitions and that of perpendicular transitions involved in the multiphoton process. Therefore, a nodal line should appear in the MRMI map along the polarization direction when $n \geq 1$, as illustrated in Fig. 4(a), where the simulated MRMI maps^{15,16} for the three kinds of two-photon dissociation processes, i.e., $\parallel + \parallel$ ($m = 2, n = 0$), $\parallel + \perp$ ($m = n = 1$), and $\perp + \perp$ ($m = 0, n = 2$) are shown. The nodal pattern should remain even when O_2^+ is prepared with its molecular axis aligned along the laser polarization direction as shown in Fig. 4(b), in which the alignment distribution is assumed to be expressed as $P_{\text{align}}(\theta) = \cos^k \theta$ with respect to the laser polarization vector. The resultant angular distribution is then expressed as $P(\theta) \cdot P_{\text{align}}(\theta)$. The index k is chosen to be $k = 6$ in the figure in order to approximately describe the fragment anisotropy observed in the MRMI map at $\lambda \sim 795$ nm [Fig. 3(a)].

The absence of a nodal line in Fig. 3 means that the electronic states coupled exclusively through parallel transitions dominate the dissociation process. The simulation of the MRMI map, in which an effect of the finite detector size^{15,16} is taken into account, shows that the observed angular distribution of the (1,0) pathway is well reproduced by the distribution function of $P(\theta) \propto \cos^k \theta$ with $k = 10(4)$ and $4(2)$ for $\lambda \sim 795$ nm and $\lambda \sim 398$ nm, respectively, which are slightly smaller than the k values for the (1,1) Coulomb explosion pathway obtained from Fig. 3, i.e., $k = 12(2)$ for $\lambda \sim 795$ nm and $k = 6(2)$ for $\lambda \sim 398$ nm. This exclusive choice of parallel transitions may be attributed to the spatial alignment of the molecular axis for the parent ions at the ionization step followed by the strong coupling among the electronic states through charge-resonance type transitions.

The parallel transitions occur among the states with a common electronic symmetry in the limit of the Hund's coupling case (a). Because O_2^+ is expected to be prepared first in either $X^2\Pi_g$ or $a^4\Pi_u$, the observed angular distribution

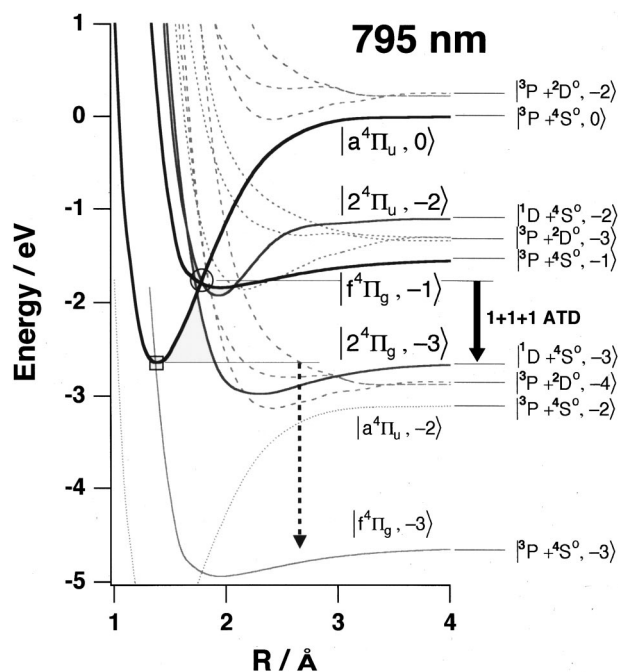


FIG. 5. The dressed-state potential curves of O_2^+ for 795 nm (1.56 eV) for the electronic states of O_2^+ correlating with the ${}^3P + {}^4S^0$, ${}^1D + {}^4S^0$, and ${}^3P + {}^2D^0$ asymptotes. For simplicity, the light-dressed state is represented by setting $N=0$, i.e., for example, the dressed states $|a^4\Pi_u, N\rangle$ and $|f^4\Pi_g, N-1\rangle$ are represented as $|a^4\Pi_u, 0\rangle$ and $|f^4\Pi_g, -1\rangle$, respectively. The dressed states involved in the coupling scheme are shown with solid lines. The other dressed states are represented with broken lines (---) for ${}^4\Pi_u$ and dotted lines (.....) for ${}^4\Pi_g$. The potential crossing point between the charge resonant states, $a^4\Pi_u$ and $f^4\Pi_g$, is indicated by an open circle. The expected released kinetic energy is represented by the length of a solid arrow. The shoulder-like feature observed at the energy of 2.0 eV is tentatively assigned to the dissociation through the three photon crossing between the $|a^4\Pi_u, N\rangle$ and $|f^4\Pi_g, N-3\rangle$ states, indicated with an open square, into the $|{}^3P + {}^4S^0, N-3\rangle$ asymptote.

suggests that the coupling among the Π electronic states plays a dominant role in the dissociation dynamics of O_2^+ . This symmetry consideration is important because it reduces significantly the number of electronic states that could be involved in the possible dissociation pathways.

C. Sequential coupling of the light-dressed states

The nuclear dynamics of molecules in intense laser fields has often been discussed in terms of light-dressed states $\{|i, N\rangle\}$ that are formed through the coupling between molecular states $\{|i\rangle\}$ and photon-field states $\{|N\rangle\}$. The interaction between molecules and the light fields is expressed as that between the dressed states, leading to potential deformation through avoided crossings. Although this dressed-state picture holds rigorously only when the light field is stationary, it can provide a clear insight into nuclear motions of molecules in the nonstationary strong laser fields.

When O_2^+ is prepared in the $a^4\Pi_u$ state, ${}^4\Pi_g$ and ${}^4\Pi_u$ electronic states are relevant to the dissociation process, since a transition moment for the transitions among the states with the same spin multiplicity is substantially larger than that for intercombinations. The interatomic potentials of the low-lying ${}^4\Pi_g$ and ${}^4\Pi_u$ electronic states of O_2^+ in the dressed picture are shown in Fig. 5 for the photon energy of 1.56 eV

($\lambda=795$ nm). The potential curves of the electronic states correlating to the ${}^3P+{}^4S^o$ and ${}^1D+{}^4S^o$ asymptotes are taken from a multireference double configuration interaction (CI) calculation by Marian *et al.*,²⁰ where the reliability of the electronic energy was estimated to be better than 0.3 eV. The deviation of the calculated dissociation energy of the $a^4\Pi_u$ state from the corresponding experimental value is only 0.03 eV.²⁰ The potential curves of the higher-lying excited states correlating to the ${}^3P+{}^2D^o$ asymptote are taken from a full valence CI calculation with a minimum-basis set by Beebe *et al.*²¹

A large transition moment between a pair of the charge resonance states²² could cause a large avoided crossing between the $|a^4\Pi_u, N\rangle$ and $|f^4\Pi_g, N-1\rangle$ potential curves. The dissociation through the (1,0) pathway at $\lambda\sim 795$ nm is thus expected to proceed dominantly from the $v\sim 6$ vibrational levels of the $a^4\Pi_u$ state near the one-photon potential crossing. Since this one-photon crossing is located in energy below the asymptotic level of the $|b^4\Pi_g, N-1\rangle$ state, i.e., $|{}^3P+{}^4S^o, N-1\rangle$, as seen in Fig. 5, this coupling does not lead directly to the dissociation. The dressed picture in Fig. 5 suggests that additional two dressed states, $|2^4\Pi_u, N-2\rangle$ and $|2^4\Pi_g, N-3\rangle$, located close to the crossing region, can make an interaction sequence $|a^4\Pi_u, N\rangle \rightarrow |f^4\Pi_g, N-1\rangle \rightarrow |2^4\Pi_u, N-2\rangle \rightarrow |2^4\Pi_g, N-3\rangle$, which is expected to occur with a sufficiently large efficiency since it proceeds through a one-photon coupling at each step.

Since the energy of the crossing between $|a^4\Pi_u, N\rangle$ and $|f^4\Pi_g, N-1\rangle$ is located above the dissociation limit of the $|2^4\Pi_g, N-3\rangle$ state, this sequential coupling of the four electronic states leads to the dissociation, which may be referred to as 1+1+1 ATD. The released kinetic energy for this dissociation pathway, represented by the length of the solid arrow in Fig. 5, is calculated to be 0.8(2) eV from the theoretical energy difference between the $|a^4\Pi_u, N\rangle - |f^4\Pi_g, N-1\rangle$ crossing and the $|{}^1D+{}^4S^o, N-3\rangle$ asymptote, which is consistent with the observed value of 1.1(1) eV, determined from the momentum distribution of O^+ in Fig. 2(a).

At $\lambda\sim 398$ nm, the dressed-state potentials (Fig. 6) are substantially different from those in Fig. 3 due to the doubled photon energy (3.12 eV). As shown in the figure, the coupling among the $a^4\Pi_u$, $f^4\Pi_g$ and $2^4\Pi_u$ states is expected to contribute to the fragmentation as in the case of $\lambda\sim 795$ nm. However, the three ${}^4\Pi_g$ states ($3^4\Pi_g$, $4^4\Pi_g$, and $5^4\Pi_g$) correlated to the ${}^3P+{}^2D^o$ asymptote, denoted hereafter as $\{^4\Pi_g\}$, may participate in place of the $2^4\Pi_g$ state which is shifted far below in energy from the interaction region. Therefore, the interaction sequence for $\lambda\sim 398$ nm can be expressed as $|a^4\Pi_u, N\rangle \rightarrow |f^4\Pi_g, N-1\rangle \rightarrow |2^4\Pi_u, N-2\rangle \rightarrow \{|^4\Pi_g\}, N-3\rangle$.

As mentioned in Sec. III B, the MRMI map of O^+ at $\lambda\sim 398$ nm [Fig. 3(b)] shows a marked difference from that observed at $\lambda\sim 795$ nm. Apart from the features for the (1,1) Coulomb explosion pathway, three pairs of crescent-like features are observed in the momentum region below 70×10^3 amu/s, with the total release energies of 0.5(1), 1.8(2), and 3.7(2) eV. The appearance of these peaks can be explained by referring to the interaction sequence of the

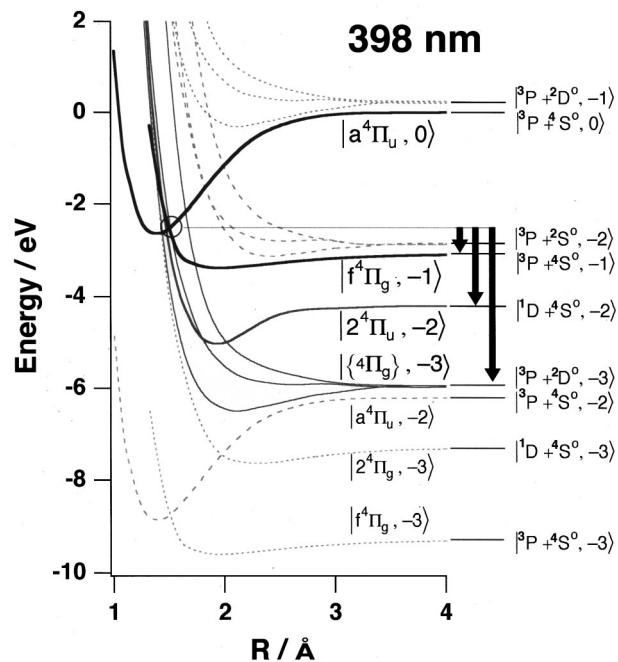


FIG. 6. The dressed-state potential curves of O_2^+ for 398 nm (3.12 eV). The expected released kinetic energies for the three fragmentation pathways are indicated by the length of the respective arrows.

dressed states represented in Fig. 6. At $\lambda\sim 398$ nm, the potential crossing between $|a^4\Pi_u, N\rangle$ and $|f^4\Pi_g, N-1\rangle$ is located above all the dressed asymptotes for the interaction sequence. Therefore, O_2^+ prepared in the $|a^4\Pi_u, N\rangle$ state undergoes dissociation into the $|{}^3P+{}^4S^o, N-1\rangle$ asymptote through the coupling with the $|f^4\Pi_g, N-1\rangle$ state at low field intensity. As the field intensity increases, it is expected that the $|2^4\Pi_u, N-2\rangle$ and $\{|^4\Pi_g\}, N-3\rangle$ states begin to participate in the dissociation process, and lead to the fragmentation into the $|{}^1D+{}^4S^o, N-2\rangle$ and $|{}^3P+{}^2D^o, N-3\rangle$ asymptotes, respectively. The released kinetic energies for these dissociation pathways represented by the length of the solid arrows in Fig. 6 are calculated to be 0.6(2), 1.7(2), and 3.6(2) eV, which are in good agreement with the corresponding observed energies (see Table I). Therefore, it is reasonable to regard that the three (1,0) peaks $\lambda\sim 398$ nm represent the dissociation into the three difference asymptotes.

As seen in Fig. 2(b), the fragments with a larger momentum appear at larger field intensities. This dependence of the peak intensities on the laser-field intensity is consistent with the above interpretation using the coupling sequence of the dressed states at $\lambda\sim 398$ nm. From the intensity variation of these three components in the 0.03–0.7 PW/cm² range, the saturation intensities were estimated to be 0.10(5), 0.13(5), and 0.18(5) PW/cm² for the peaks observed at 0.5, 1.8, and 3.7 eV, respectively.

The transition moment μ of the $f^4\Pi_g - a^4\Pi_u$ charge resonance transition was calculated²⁰ to be $\mu=0.5$ a.u. at the internuclear distance $R=1.6$ Å, where the $|a^4\Pi_u, N\rangle$ and $|f^4\Pi_g, N-1\rangle$ states cross with each other at $\lambda\sim 398$ nm (see Fig. 5). A slightly larger transition moment, $\mu=0.8$ a.u. was obtained at $R=1.9$ Å for the crossing at $\lambda\sim 795$ nm (Fig. 4).

These values are smaller by a factor of 2–3 than those expected from the formula ($\mu=R/2$),²² i.e., $\mu=1.5$ and 1.8 a.u. for $R=1.6$ and 1.9 Å, respectively, because of the configuration mixing of the $f^4\Pi_g$ state with other electronic states.²⁰ Then, the magnitude of the energy gap at the avoided crossing between the charge resonance pair is estimated to be on the order of $\mu I^{1/2}\sim 1$ eV at the saturation intensity ($I\sim 0.2$ PW/cm²). Accordingly, an energy gap at a three-photon crossing is expected to be much smaller in the present case. Indeed, the energy gap between the $|a^4\Pi_u, N\rangle$ and $|f^4\Pi_g, N-3\rangle$ states is calculated to be only 0.03 eV at 0.2 PW/cm² for $\lambda\sim 795$ nm. As shown in Fig. 5, the dissociation through this three-photon gap marked by a square proceeds by passing the $|a^4\Pi_u, N-2\rangle-|f^4\Pi_g, N-3\rangle$ crossing point diabatically, resulting in the formation of the O^+ ions with the kinetic energy of 2.0(3) eV, which is represented by a broken arrow. The shoulder-like structure at 2.0 eV [see Fig. 2(a)] may be ascribed to this diabatic passage.

More detailed discussion of the dissociation pathways through an interaction sequence in intense laser fields would become possible if more precise large-scale *ab initio* calculations are performed to derive the transition moments between the quartet states of O_2^+ as well as their potential energy curves.

D. Comparison with previous studies

Normand *et al.*¹⁴ observed a diffuse peak in the TOF spectra of O^+ at $\lambda\sim 610$ nm, 0.05 PW/cm², in which two overlapping components were identified with released kinetic energies of ~ 0.7 and 1.4 eV. When the present multiple coupling model is adopted, the two interaction sequences, $|a^4\Pi_u, N\rangle\rightarrow|f^4\Pi_g, N-1\rangle\rightarrow|2^4\Pi_u, N-2\rangle\rightarrow|2^4\Pi_g, N-3\rangle$ and $|a^4\Pi_u, N\rangle\rightarrow|f^4\Pi_g, N-1\rangle\rightarrow|2^4\Pi_u, N-2\rangle\rightarrow\{|^4\Pi_g\}, N-3\rangle$, give the release energies of 0.7(2) and 2.1(2) eV, respectively. Although the latter is slightly larger than the observed value by 0.7 eV, the difference between the observed and calculated peak position is rather small (~ 18 ns) in the TOF spectra as compared with the width of the observed diffuse peak (~ 140 ns).

The consistent interpretation of the experimental kinetic energies of O^+ at three different wavelengths assures an applicability of the present model of a sequential coupling of the dressed states within the $^4\Pi$ manifold and suggests that O_2^+ ion populated in the $X^2\Pi_g$ state affords only a small contribution to the dissociation process. This may be explained by assuming that the $X^2\Pi_g$ state is prepared in the low vibrational levels after the ionization step, located far below (~ 6 eV) the $^3P+^4S^o$ dissociation limit. Since the potential crossing between the charge resonance states, $|X^2\Pi_g, N\rangle$ and $|A^2\Pi_u, N-1\rangle$, is located ~ 3 and ~ 1.5 eV above these vibrational levels at $\lambda\sim 795$ and 398 nm, respectively, the one-photon coupling could not contribute to the dissociation process to a large extent.

On the other hand, the present model within the $^4\Pi$ manifold can only account for one of the three components observed at a shorter wavelength at $\lambda\sim 305$ nm¹⁴ as shown in Table I. The other two components with lower kinetic ener-

gies could be assigned to the dissociation starting from the $X^2\Pi_g$ state. When the coupling among the doublet Π states at $\lambda\sim 305$ nm is treated in the same manner as described above, the released energy corresponding to the dissociation into the $|^3P+^2P^0, N-3\rangle$ from the crossing between $|X^2\Pi_g, N\rangle$ and $|A^2\Pi_u, N-1\rangle$ states is calculated to be 1.3(3) eV, which is in good agreement with 1.04 eV, one of the remaining two observed values. In order to explain the lowest energy component at 0.52 eV, it may be necessary to take into account additional interactions between the doublet and quartet states²³ and/or the resonance effects^{23,24} in the ionization step that could modulate the initially prepared vibrational distribution in the bound states.

IV. SUMMARY

Based on the MRMI measurements of the fragment O^+ ion, the photodissociation process, $O_2^+\rightarrow O^++O$, in intense laser fields (~ 1 PW/cm², $\lambda\sim 795$ and 398 nm) was investigated. The covariance map measurements were performed with high momentum resolution to assign securely the dissociation pathways. It was found from the anisotropic distribution of O^+ along the laser polarization vector that the parallel transitions dominate the fragmentation processes, which could be attributed to an anisotropic preparation of the parent ions at the ionization step followed by the strong coupling among the electronic states through charge-resonance type transitions. The total kinetic energy release of O^+ for both 795 and 398 nm was interpreted consistently by a sequential coupling model of light-dressed potential curves of O_2^+ in the quartet Π state manifold rather than in the doublet Π state manifold. The consistent interpretation of the experimental kinetic energies of O^+ at the two different wavelengths shows that the dissociation dynamics of O_2^+ in intense laser fields of ~ 1 PW/cm² can be interpreted within the framework of the dressed state picture by considering the light-induced multiple coupling among molecular electronic states.

ACKNOWLEDGMENT

The present work was supported by the CREST (Core Research for Evolutionary Science and Technology) fund from Japan Science and Technology Corporation.

- ¹A. D. Bandrauk, *Molecules in Laser Fields* (Dekker, New York, 1993).
- ²A. Giusti-Suzor, F. H. Mies, L. F. DiMauro, E. Charron, and B. Yang, *J. Phys. B* **28**, 309 (1995).
- ³T. Zuo and A. D. Bandrauk, *Phys. Rev. A* **52**, R2511 (1995).
- ⁴I. Kawata, H. Kono, and Y. Fujimura, *J. Chem. Phys.* **110**, 11152 (1999).
- ⁵K. Codling and L. J. Frasinski, *J. Phys. B* **26**, 783 (1993).
- ⁶B. Sheehy and L. F. DiMauro, *Annu. Rev. Phys. Chem.* **47**, 463 (1996).
- ⁷C. Cornaggia, *Phys. Rev. A* **54**, R2555 (1996).
- ⁸W. A. Bryan, J. H. Sanderson, A. El-Zein, W. R. Newell, P. F. Taday, and A. J. Langley, *J. Phys. B* **33**, 745 (2000).
- ⁹A. Hishikawa, A. Iwamae, and K. Yamanouchi, *Phys. Rev. Lett.* **83**, 1127 (1999).
- ¹⁰A. Hishikawa, A. Iwamae, and K. Yamanouchi, *J. Chem. Phys.* **111**, 8871 (1999).
- ¹¹J. H. Sanderson, A. El-Zein, W. A. Bryan, W. R. Newell, A. J. Langley, and P. F. Taday, *Phys. Rev. A* **59**, R2567 (1999).
- ¹²S. Liu, A. Hishikawa, A. Iwamae, and K. Yamanouchi, in *Advances in Multiphoton Processes and Spectroscopy*, edited by Y. Fujimura and R. J. Gordon (World Scientific, Singapore, 2001), Vol. 13, p. 182.

- ¹³L. J. Frasinski, K. Codling, and P. A. Hatherly, *Science* **46**, 1029 (1989).
- ¹⁴D. Normand, C. Cornaggia, J. Lavancier, J. Morellec, and H. X. Liu, *Phys. Rev. A* **44**, 475 (1991).
- ¹⁵A. Hishikawa, A. Iwamae, K. Hoshina, M. Kono, and K. Yamanouchi, *Chem. Phys.* **231**, 315 (1998).
- ¹⁶A. Iwamae, A. Hishikawa, and K. Yamanouchi, *J. Phys. B* **33**, 223 (2000).
- ¹⁷C. Guo, M. Li, and G. N. Gibson, *Phys. Rev. Lett.* **82**, 2492 (1999).
- ¹⁸G. Herzberg and K. P. Huber, *Molecular Spectra and Molecular Structure IV: Constants of Diatomic Molecules* (Van Nostrand Reinhold, New York, 1979).
- ¹⁹R. N. Zare, *Mol. Photo Chem.* **4**, 1 (1972).
- ²⁰C. Marian, R. Marian, S. D. Peyerimhoff, B. A. Hess, R. J. Buenker, and G. Seger, *Mol. Phys.* **46**, 779 (1982).
- ²¹N. H. F. Beebe, E. W. Thulstrup, and A. Andersen, *J. Chem. Phys.* **64**, 2080 (1976).
- ²²R. S. Mulliken, *J. Chem. Phys.* **7**, 20 (1939).
- ²³B. L. G. Bakker, D. H. Parker, P. C. Samartzis, and N. Kitsopoulos, *J. Chem. Phys.* **112**, 5654 (2000).
- ²⁴B. Walker, M. Saeed, T. Breeden, B. Yang, and L. F. DiMauro, *Phys. Rev. A* **44**, 4493 (1991).